Geotech Geol Eng (2019) 37:1453–1467
https://doi.org/10.1007/s10706-018-0699-0

ORIGINAL PAPER

Using Finite Element Strength Reduction Method for Stability Analysis of Geocell-Reinforced Slopes

Mohammad Reza Arvin · Amir Zakeri · Mostafa Bahmani Shoorijeh

Received: 30 May 2018 / Accepted: 10 September 2018 / Published online: 12 September 2018

Abstract Widespread application of geocells in practice, especially in slope stabilization, is mainly derived from the strengthening features they display in excess of membrane effect of planar geosynthetics. On the ground where geocells are in the shape of honeycombs, a three dimensional model and analysis provides a relatively more precise insight into the behavior of structures reinforced with them compared to the prevalent 2D means of slope stability analysis or methods taking the geocell layer as an equivalent soil layer. The three dimensional stability of geocell-reinforced slopes was investigated using strength reduction method (SRM) in the present paper. Both the geocells and their infill and surrounding soils were taken into account. Since ABAQUS is not provided with built-in ability of analysis by SRM, a SRM stepped procedure was adopted herein to determine FS by this finite element software. As the next step, using the aforementioned techniques, effects of some leading factors contributing to the stability of geocell-reinforced slopes such as geocell placement, pattern of multilayer reinforcement and number of geocell layers were evaluated thoroughly. Reliability of the applied stepped SRM procedure was verified in advance using the available results of a previously 3D- SRM slope stability analysis.

Keywords Strength reduction Method · Slope stability · Geocell · Safety factor · ABAQUS

M. R. Arvin (✉)
Civil Engineering Department, Fasa University, Bahmanbeigi Square, Moheb Blvd, P.Box: 7461781189, Fasa, Iran
e-mail: m.r.arvin@fasau.ac.ir

A. Zakeri
Department of Civil Engineering, Islamic Azad University, Estahban, Iran
e-mail: amir.zakeri@yahoo.com

M. Bahmani Shoorijeh
Zachry Department of Civil Engineering, Texas A&M University, College Station, TX, USA
e-mail: bahm64@tamu.edu

1 Introduction

Ease of construction, durability against erosion, high quality of performance and cost-effectiveness has made the enhancement of the stability of slopes by means of geosynthetics popular during the recent decades. Contrary to planar geosynthetics such as geogrid, geotextile and geocomposite, geocell has a honeycomb three dimensional structure that makes its contribution to soil improvement more complicated. Superiority of geocell on planar and randomly distributed geosynthetics was indicated by Dash et al. (2004) through some model tests on strip foundations. Three different mechanisms, namely load dispersion, confining effect and membrane effect were identified to be responsible for increase in the

bearing capacity and decline in the settlement of geocell-reinforced foundations (Mandal and Gupta 1994, Zhang et al. 2010). Large scale triaxial tests indicate that the embedment of geocell adds an apparent cohesion to the soil strength property while the soil internal friction is just marginally affected (Bathurst and Karpurapu 1993). A variety of factors have been found to affect the behavior of structures reinforced with geocells. Most of the corresponding findings are resulted from model tests on reinforced foundations. Effects of such variables as geocell width (Dash et al. 2003a, b; Tafreshi and Dawson 2012; Dash et al. 2001; Dash et al. 2007), depth of geocell layers (Dash et al. 2007; Sitharam et al. 2005), geocell height (Mandal and Gupta 1994; Dash et al. 2003b, 2007; Sitharam et al. 2005), geocell material (Dash et al. 2001), pocket shape (Dash et al. 2001), infill material (Hegde and Sitharam 2015) and infill density (Sireesh et al. 2009) have been explored through empirical means. A detailed review on the recent empirical studies on geocell-reinforced soil can be seen in Hegde (2017) and Biswas and Krishna (2017).

Due to the complexity of geocell simulation in numerical models, equivalent soil layers are preferred and applied to the geocell mattress by some researchers (Hegde and Sitharam 2015; Rajagopal et al. 1999; Madhavi Latha and Rajagopal 2007; Latha et al. 2008). In this context, stability of geocell-reinforced slopes was investigated by Mehdipour et al. (2013, 2017) simulating the geocell layer as an equivalent beam element. In order to account for the whole complexities of the geocell-reinforced structures, both geocell and infill soil should be modeled in a numerical analysis. However, only a few such studies are available in the literature (Hegde and Sitharam 2015; Han et al. 2008; Leshchinsky and Ling 2013a, b).

Generally, engineers prefer to perform a 2D analysis for the assessment of the slope's behavior and stability because of its simplicity and ease of understanding. Besides, a 2D analysis always gives a conservative estimation of the factor of safety in comparison to the 3D analysis. However, in practice, due to irregularities in topography, loading and material, most situations do not meet the plain strain conditions. In this regard, in line with considering the fact the 3D factor of safety is always greater than 2D one and consequently more cost-effective, sometimes scrutiny of the slopes by a 3D method becomes inevitable, especially when it comes to financial issues. On the ground of the honeycomb structure of the geocell, only a 3D analysis is able to reflect the true behavior of a geocell-reinforced slope even if everything including geometry, loading, material, etc. can be regarded as symmetric.

Most of the 3D slope stability approaches have been developed by generalization of the limit equilibrium 2D methods (Hungr 1987; Lam and Fredlund 1993; Chen et al. 2003; Cheng and Yip 2007; Ahmed et al. 2012). In addition to inability of limit equilibrium methods to satisfy all equilibrium terms, shape of the slip surface must be assumed a priori and is not precisely predictable using these techniques (Wong 1984). These drawbacks have been overcome to a great extent in the strength reduction method (SRM).

SRM is a powerful approach to evaluate the stability of slopes. This method obtains the safety factor by gradually decreasing the soil strength parameters until a predefined failure criterion is met. Both equilibrium and yield conditions are satisfied simultaneously and the shape of the slip surface is specified almost precisely in the end. SRM was pioneered by Zienkiewicz et al. (1975) for associated and nonassociated soil structures. Ever since, strength reduction method has been widely improved in different aspects. SRM is a general term and different approaches to this method are characterized by the standard according to which they finalize the calculation and settle the factor of safety. In this regard, nodal displacement method (Zienkiewicz et al. 1975; Donald and Giam 1988) is the earliest standard and simplest technique for FS inspection. In this method, displacement versus reduction factor (i.e. safety factor) for some nodes, preferably in the failure region, is drawn and a point on the curve associated with a sharp drop in displacement will be defined. The reduction factor corresponding to the prementioned point can be regarded as the safety factor. In addition to the nodal displacement benchmark, other scales such as shear strain failure criterion (Matsui and San 1992), divergence of the nonlinear analysis (Griffiths and Lane 1999; Faheem et al. 2003; Griffiths and Lu 2005; Tschuchnigg et al. 2015) and arc-length technique (Song 1997) have been developed so far to specify the FS and estimate the slip surface of the slopes. SRM based on nonlinear divergence technique is incorporated in some well-known commercial

computer software such as FLAC2D, FLAC3D and Phase2. For instance, finite element software Plaxis is able to perform strength reduction analysis using arc-length method.

While most of the available SRM-related researches have been devoted to two dimensional unreinforced slopes (Zienkiewicz et al. 1975; Donald and Giam 1988, Matsui and San 1992; Griffiths and Lane 1999; Faheem et al. 2003; Griffiths and Lu 2005; Tschuchnigg et al. 2015; Song 1997; Cheng et al. 2007), some researchers have investigated the 3D stability of slopes using this technique (Ugai and Leshchinsky 1995; Griffiths and Marquez 2007; Deng et al. 2007; Wei et al. 2009). SRM has also been applied to evaluate the safety of reinforced slopes. Cai and Ugai (2000) applied SRM to study the effects of the contributing parameters to the stability of slopes reinforced with piles. Later, they used SRM in the analysis of anchor-reinforced slopes (Cai and Ugai 2003). Stability of pile-reinforced slopes was also investigated by Wei and Cheng (2009), utilizing SRM. Stability of nailed slopes has also been studied by strength reduction method (Lin et al. 2013; Wei and Cheng 2010; Rawat and Gupta 2016). Furthermore, Mehdipour et al. (2013) simulated geocell layers as the equivalent beam elements and studied the effects of some factors such as geocell placement and the number of geocell layers carrying out 2D-SRM analyses by FLAC2D. To the best of the author's knowledge, there is still no available research work conducted on the 3D-SRM analysis of geocell-reinforced slopes.

In this paper, stability of slopes reinforced by geocell layers is investigated using strength reduction method through three dimensional finite element analysis. To do so, ABAQUS software is used for numerical modeling and analysis. Nodal displacement technique has been utilized to determine the factor of safety. In order to obtain the most possible accurate FS, a stepped solution procedure is adopted to ensure that the selected nodes, for failure examination, are located in the collapsed region. Firstly, validity of the proposed technique is verified through comparison to some available results of 3D-SRM analysis on unreinforced slopes. Then, the effects of the geocell depth, the number of geocell layers and the multilayer geocell pattern are investigated.

2 SRM Using ABAQUS

In the present study, stress reduction method (SRM) is employed to determine the safety factor of slope against instability. Generally, the factor of safety of an earth slope composed of a soil with cohesion (c) and internal friction angle φ is defined as:

$$\mathrm{FS} = \frac{c}{c_m} = \frac{\tan\varphi}{\tan\varphi_m} \tag{1}$$

where c_m and φ_m are the mobilized cohesion and friction angle respectively. Hence, FS can be determined provided that the values of c_m and φ_m are specified by some means. Based on the strength reduction method, cohesion and internal friction angle of the soil are reduced gradually and simultaneously at the same rate to the point of slope instability. The reduced cohesion ($c_{reduced}$) and internal friction angle ($\varphi_{reduced}$) are in essence the mobilized strength parameter of the soil and the rate by which c and φ are decreased is, by definition, the factor of safety FS. Therefore, according to the SRM, the factor of safety may be redefined as follows:

$$\mathrm{FS} = \frac{c}{c_{reduced}} = \frac{\tan\varphi}{\tan\varphi_{reduced}} \tag{2}$$

As indicated in the introduction section, some computer software such as FLAC2D, FLAC3D, Phase2 and Plaxis entail built-in strength reduction ability. These kinds of software automatically reduce the soil strength parameters and stop the analysis where their defined instability criteria is held. ABAQUS is a FEM-based versatile computer software used in diverse engineering areas. Since the strength reduction capability is generally applied to geotechnical problems, naturally ABAQUS has not been equipped with such an ability. Thus, in order to find FS via ABAQUS, one needs to develop a technique to gradually alter the soil strength parameters and find the cohesion and internal friction angle corresponding to an appropriately defined benchmark for failure. Then, FS can be identified using Eq. 1. The following nodal displacement based procedure is developed in this study to calculate the factor of safety using the outputs of ABAQUS:

1. In order to add the quality of variability in material properties to the software, soil strength properties are defined as temperature dependent. This way,

for a single material, numerous values of cohesion and internal friction angle can be defined, each of which is associated with its corresponding value of temperature. Gradual reduction of strength parameters is sorted out in line with the temperature rise. Hence, the software performs an analysis in accordance with the aforementioned organized material properties.

2. The analysis consists of several steps depending on the construction stages and the number of reduction levels in strength parameters. Performing static general analysis for all the reduction phases is significantly time consuming. Therefore, as a solution to reduce the analysis time, explicit dynamic analysis can be performed instead of static general analysis for complicated models, provided that the model is given enough time (t) at each step to reach the same solution as the static responses. Steps of the present analysis are made up of gravity loading, surface loading and the proceeding strength reduction phases. Therefore, the total time steps devoted to the analyses equals the number of steps times t.
3. The slope composed of the temperature dependent soil is analyzed and stress, strain and displacement fields are determined for each temperature level corresponding to reduced strength parameters.
4. Scrutinizing the maximum principal plastic strain contours or shadings, the failure surface can be recognized. A reference point is defined. For a symmetrical model like what is under investigation here, the reference point is taken at the middle of the failure surface toe.
5. Horizontal displacement versus time is drawn for the reference point. A time on the graph at which, there is a sudden increase in the total displacement is regarded as the failure outburst. This time is associated with its corresponding reduced cohesion and internal friction angle so that the factor of safety can easily be determined using Eq. 2.

The proposed technique above is similar to Nodal displacement method. The only difference is that unlike the conventional nodal displacement approach, selected node is not assumed from the beginning and is specified after the accomplishment of the analysis when the slip surface can be recognized with acceptable accuracy. Preferably, the selected node to sketch time-displacement curve is considered at the toe of the slip surface.

It should be noted that since the displacement–time graph is not a bilinear curve in general, the time associated with the dramatic increase in displacement cannot be defined straightforwardly. To overcome this issue, the intersection of lines tangential to the two relatively straight parts of the curve before and after the drop point is considered as the target point and its corresponding coordinates (time and displacement) are extracted for further analysis.

3 Verification

In order to examine the reliability of the proposed method, it is verified with the results of three dimensional strength reduction analysis performed by Wei et al. (2009). Hence, a three dimensional model of slope employed by Wei et al. (2009) was simulated in Abaqus as well. Geometrical properties and a three dimensional view of the model are illustrated in Fig. 1.

The model is a 45° inclined slope, 6 m in height resting on a 24 m deep foundation bed. Boundaries of the model are placed far enough to avoid interference of the boundaries in the slope behavior. Sensitivity analyses showed that taking lengths of the model in front of the slope (L_f) and at the back of the slope (L_b) equal to 24 m and 30 m respectively ensures negligible boundary effects for both reinforced and unreinforced situations (Fig. 1). Vertical boundaries are free to move up and down and are banned from lateral movement while the base boundary is totally fixed. Sensitivity analysis on both reinforced and unreinforced models were performed to choose the maximum possible size of the elements. It followed that taking relatively coarse elements at parts away from the slope and stress concentration had marginal effect on the results. Therefore, the model was meshed so that elements located at or near the slope and the local load placement are much finer (0.14 m $<$ element size $<$ 1.06 m) than elements that belong to the other parts of the model, in particular in vicinity of the left and right boundaries where maximum element size up to 10 m is shown to have negligible impact on the results. Eight-node hexahedral elements were employed to generate the mesh of soil mass. Soil is assumed to be a homogeneous, isotropic material

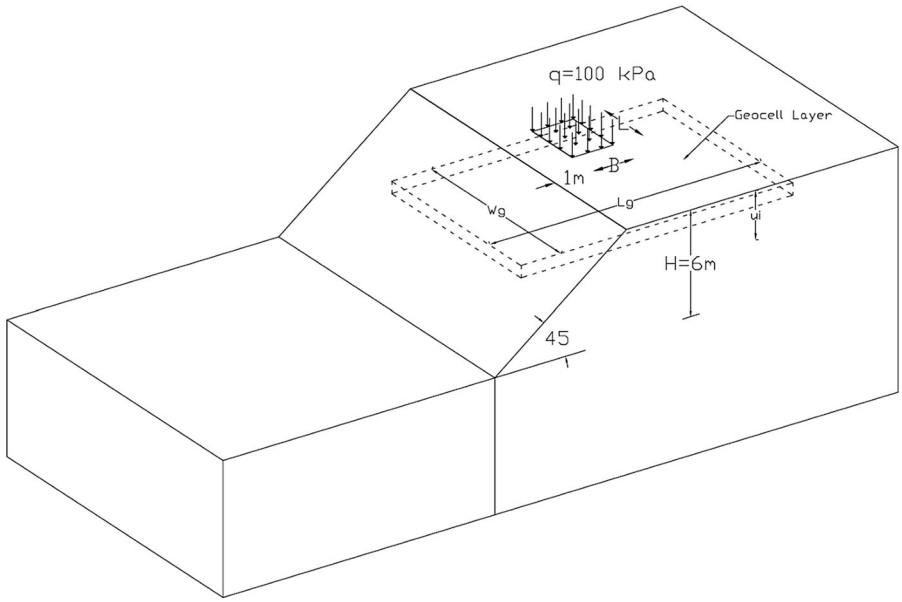

Fig. 1 Schematic view of the slope model considered in the present study

complying with the Mohr–Coulomb failure criterion and associated flow rule. The slope is subjected to a rectangular load, L in length and B in width, which is located a 1 m distance from the slope's edge (Fig. 1). Wei et al. took the intensity of load as 100 kPa and assumed B equal to 2 m, and analyzed the model for a range of load lengths to see the effect of L/B on the factor of safety. They determined the factor of safety by limit equilibrium method (LEM) and strength reduction method (SRM) separately. The soil properties used by Wei et al. (2009) are presented in Table 1.

According to the step 1 of the solving procedure described in the theory section, Mohr–Coulomb criterion were defined and assigned as a temperature dependent constitutive model. Analyses proved that allocating 5 s to each step of the explicit dynamic analysis steps, leads to outputs identical to the general static analysis. Therefore, each step of analyses consisting of gravity loading, surface load enforcement and c-φ reduction steps were given a 5 s time interval. Table 2 outlines the way soil was introduced to the ABAQUS software.

As Table 2 indicates, each time step corresponds to a specified c, ϕ and FS. It should be noted that dilation angle ψ, that was initially equal to ϕ, was being changed at the same rate as the friction angle through the solving process. The model developed in the present study was subjected to the prescribed loadings and analyzed for the material conditions defined in Tables 1 and 2. Figure 2 illustrates the displacement of the reference point, here on the toe of the slope, versus the analysis time for L/B = 2. As Fig. 2 suggests, there is a drastic growth in the displacement of the reference point at t = 28 s. Referring to Table 2, the corresponding FS is figured 1.65.

Results of the analyses by the present method following the step by step procedure described in the previous section, are depicted in Table 3. As Table 3 indicates, while the results of the present study are always slightly higher than SRM outputs of Wei et al., with maximum difference of 4.4%, they are satisfactorily in compliance with each other.

The verified results presented in the Table 3 prove that the stepped analysis procedure introduced in the

Table 1 Properties of soil assumed for verification

Density (kN/m^3)	Cohesion (kN/m^2)	Friction angle (°)	Young's modulus (MPa)	Poisson ratio
20	20	20	20	0.35

Table 2 Summary of the Mohr–Coulomb soil introduced to the software

Step name	Step no.	Temp (° cen)	Time (s)	c (kN/m^2)	φ (°)	FS
Gravity loading	1	35	0–5	20	20	1
Load enforcement	2	35	6–10	20	20	1
c-φ analysis	3	35	11–15	20	20	1
c-φ reduction	4	36	16	19.05	19.20	1.05
			17	18.18	18.31	1.10
			18	17.39	17.56	1.15
			19	16.67	16.87	1.20
			20	16.00	16.23	1.25
	5	37	21	15.38	15.64	1.30
			22	14.81	15.09	1.35
			23	14.29	14.57	1.40
			24	13.79	14.09	1.45
			25	13.33	13.64	1.50
	6	38	26	12.90	13.21	1.55
			27	12.50	12.82	1.60
			28	12.12	12.44	1.65
			29	11.76	12.08	1.70
			30	11.43	11.75	1.75
	7	39	31	11.11	11.43	1.80
			32	10.81	11.13	1.85
			33	10.53	10.84	1.90
			34	10.26	10.57	1.95
			35	10.00	10.31	2.00
	8	40	36	9.76	10.07	2.05
			37	9.52	9.83	2.10
			38	9.30	9.61	2.15
			39	9.09	9.39	2.20
			40	8.89	9.19	2.25
	9	41	41	8.70	8.99	2.30
			42	8.51	8.80	2.35
			43	8.33	8.62	2.40
			44	8.16	8.45	2.45
			45	8.00	8.28	2.50
	10	42	46	7.84	8.12	2.55
			47	7.69	7.97	2.60
			48	7.55	7.82	2.65
			49	7.41	7.68	2.70
			50	7.27	7.54	2.75
	11	43	51	7.14	7.41	2.80
			52	7.02	7.28	2.85
			53	6.90	7.15	2.90
			54	6.78	7.03	2.95
			55	6.67	6.92	3.00

Table 2 continued

Step name	Step no.	Temp (° cen)	Time (s)	c (kN/m^2)	φ (°)	FS
	12	44	56	6.56	6.81	3.05
			57	6.45	6.70	3.10
			58	6.35	6.59	3.15
			59	6.25	6.49	3.20
			60	6.15	6.39	3.25
	13	45	61	6.06	6.29	3.30
			62	5.97	6.20	3.35
			63	5.88	6.11	3.40
			64	5.80	6.02	3.45
			65	5.71	5.94	3.50

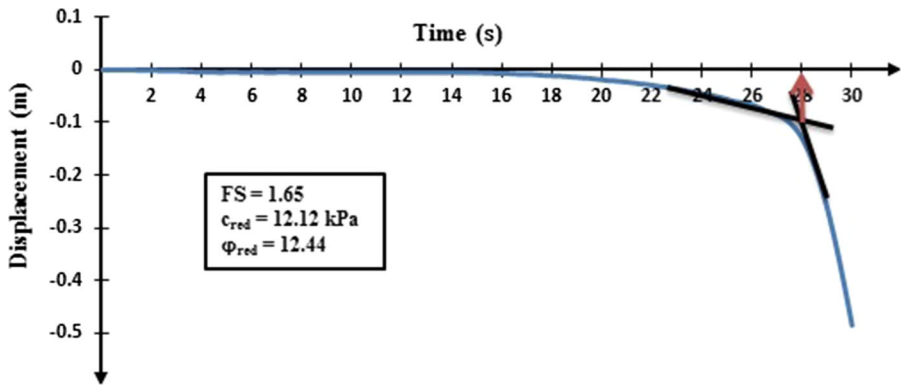

Fig. 2 Displacement versus analysis time of the reference point (slope toe) for β = 45° and L/B = 2

Table 3 Factor of safety for different L/B

L/B method	0	1	2	4	6	8	10
SRM (Wei et al. 2009)	1.82	1.71	1.60	1.41	1.33	1.30	1.26
SRM (present study)	1.90	1.75	1.65	1.45	1.40	1.35	1.30

theory section can be trusted to estimate the FS of the geocell-reinforced slopes.

4 Problem Definition

4.1 Geometry, Boundary Conditions and Loading

In order to compare the results of reinforced slopes with the corresponding unreinforced ones and for convenience, the same configuration as described in Sect. 3 was utilized for verification and utilized to study the geocell-reinforced slopes. i.e. geometrical and boundary conditions as well as soil properties were assumed to be the same as the unreinforced model. All analyses were performed assuming L/B = 4 and q = 100 kPa.

4.2 Geocell Properties

A diamond shape pocket with large and small diameter equal to 40 cm and 50 cm respectively was assumed for geocell layer and modeled in Abaqus using linear quadrilateral shell elements. As illustrated in Fig. 3, depth and sides of the geocell are supposed to be 20 cm and 32 cm respectively.

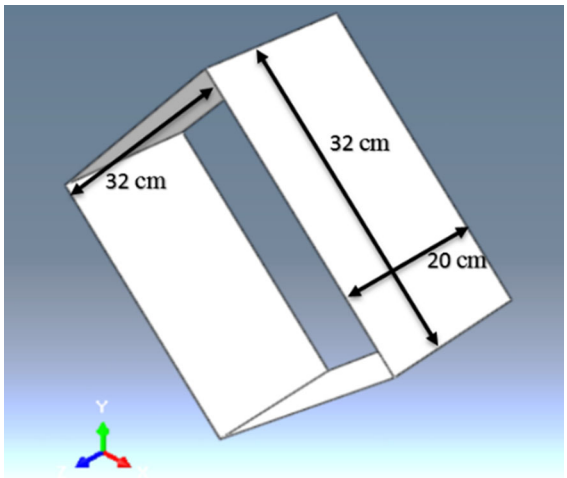

Fig. 3 Geometrical properties of the geocell pocket used in the present study

Geocells were assumed to behave isotopically and elastically which can be introduced by two parameters, elastic modulus and Poisson ratio. TherExcept for Poisson ratio, other material properties of geocell are assumed the same as those used by Leshchinsky and Ling (2013a, b) as shown in Table 4.

In addition, in the interface between soil and geocell walls, full cohesion and friction are assumed to be mobilized.

Depth of the first geocell layer, from the ground surface to the top of the reinforcing mattress, is denoted by u_1 as illustrated in Fig. 1. In case the slope is reinforced with more than one geocell layer, depth of the ith geocell layer is denoted by u_i and the distance between two successive layers is assumed to be a constant defined by s (Fig. 1). In general, width and length of the geocell layers can be different (smaller) from the corresponding measures of the model and are denoted by W_g and L_g respectively, as Fig. 1 shows.

Table 4 Material properties of geocell

Density (kN/m^3)	Elastic modulus (MPa)	Poisson ratio
15	2070	0.4

5 Results and Discussions

Effects of a variety of factors contributing to the behavior of geocell-reinforced slopes were investigated through analyses on the models introduced in the previous section. These factors include number of geocell layers, placement of the geocell layers and size of geocells mattresses. In the following, the findings of the current study will be presented.

5.1 Effects of Distribution Pattern of Geocell Layers

Arrangement of the reinforcing elements in reinforced structures plays a crucial role in their behavior and stability. It is equally significant for man-made structures, such as geocell-reinforced slopes, where reinforcement is performed over the course of construction. An optimum reinforcement arrangement may be achieved by considering possible distribution patterns. To do so, effects of different distribution of single and multiple (double and triple) geocell layer(s) over the slope height were investigated by finding the solution to some problems.

5.1.1 Single Geocell Layer

A 30 m × 12 m geocell mattress (W_g = 30 m and L_g = 12 m) as illustrated in Fig. 4 was embedded in different depths (u_1) to see the effect of the placement of a single geocell layer on the stability of slopes. The geocell layer was planted once in the top of the slope (u_1 = 1 m), once in the middle height of the slope (u_1 = 3 m) and once in the bottom of the slope (u_1 = 5 m).

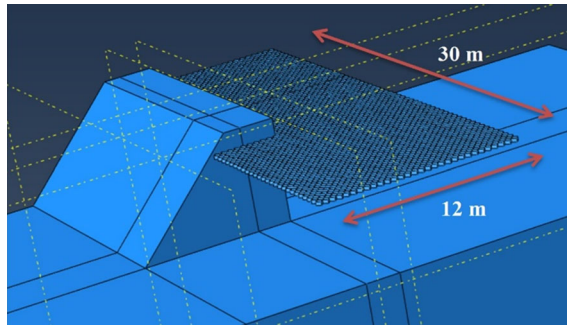

Fig. 4 A 3D section of a slope reinforced with a single geocell layer

Following the analysis, an appropriate reference point was picked considering the shape of the failure surface. While the slip surface was observed to cross the toe of the slopes reinforced at top and mid height, the failure surface existed just above the goecell layer for the bottom-reinforced slope. Hence, the reference point for the first two former cases was considered on the toe and for the latter situation on the top of the geocell layer. The FS were calculated thereafter for each case inspecting the displacement–time graph of the associated reference point. Figures 5, 6 and 7 show the failure surface (middle section view) and displacement–time graph corresponding to each case.

Factor of safety was found to be 2.05, i.e. 24.2% increase compared to unreinforced situation, for the slope reinforced in the top part as Fig. 5b indicates. Besides, slip surface is formed below the reinforcing layer and intersects the slope toe (Fig. 5a). Placing the geocell layer in the mid height led to a decline in the FS (FS = 1.85) compared to the top geocell installation as depicted in Fig. 6b. Analogous to top reinforcement, the slip surface appears to be formed below the reinforcement and passes through the slope toe (Fig. 6a). Comparison of the Fig. 7 with Figs. 5 and 6 reveals that the depth of the placement has a reverse effect on the factor of safety. That is, the movement of the geocell layer from top to the bottom of the slope has resulted in a decrease in FS from its maximum amount for top geocell (FS = 2.05) to the lowest value FS = 1.75 for the bottom geocell reinforcement. As Fig. 7a indicates, reinforcement of slopes in the bottom part leaves a large mass of unreinforced soil above the reinforcement layer vulnerable to failure so that slip surface tends to be captured in the unreinforced part rather than being affected directly by the geocell layer. Nevertheless, geocell mattress performs analogous to a stiff bed and shifts the slip surface higher than that of the unreinforced case. That is, geocell layer embedded in the lower region improves the stability by shrinking the unreinforced mass of the slope.

5.1.2 *Double and Triple Geocell Layers*

Strengthening of the slopes with two layers of reinforcement was also investigated. The same placement of the top and the bottom reinforcement discussed earlier were picked as well for the case of double layer reinforcement. That is, u_1 = 1 m and u_2 = 5 m as shown in Fig. 8. As Fig. 8 indicates, for double layer reinforcement, slip surface is captured between the two reinforcing layers and passes right above the bottom layer. In fact, the bottom reinforcement stiffening role ceases the development of the failure surface into and beneath the geocell layer. Factor of safety was calculated 2.7 which shows around 63.6% and 32% increase compared to the unreinforced slope and the single layer top-reinforcement (the optimal case among single layer reinforced slopes) respectively.

It is important to find out which arrangement results in the optimum stability when multiple layers of geocell are supposed to be used. To do so, three layers of geocell were distributed in three different patterns across the slope height. The depth of the first layer (u_1) and the distance between the two underlying layers (second and third layers) were adjusted in a way that top-inclined pattern (u_1 = 1 m, s = 1.5 m), equally

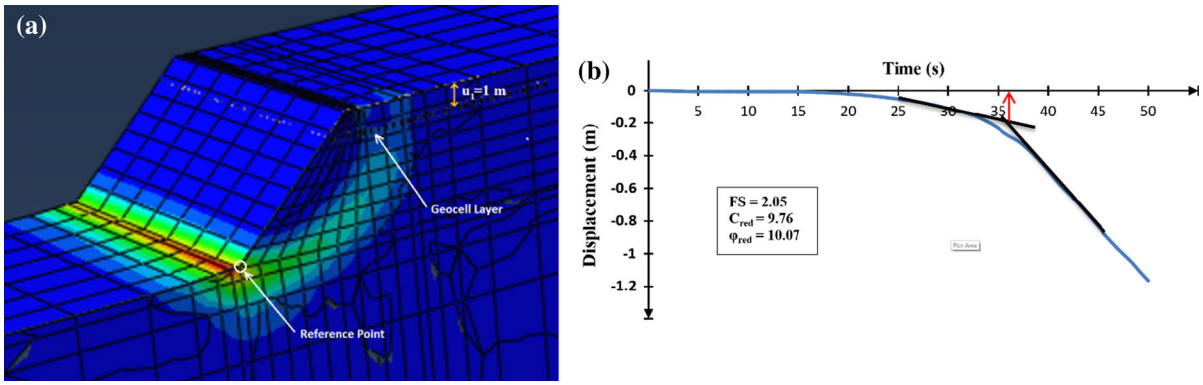

Fig. 5 Outputs of SRM analysis on the slope with β = 45° and H = 6 m, reinforced on top (u_1 = 1 m). **a** A 3D section showing the geocell layer placement and slip surface. **b** Displacement–time graph

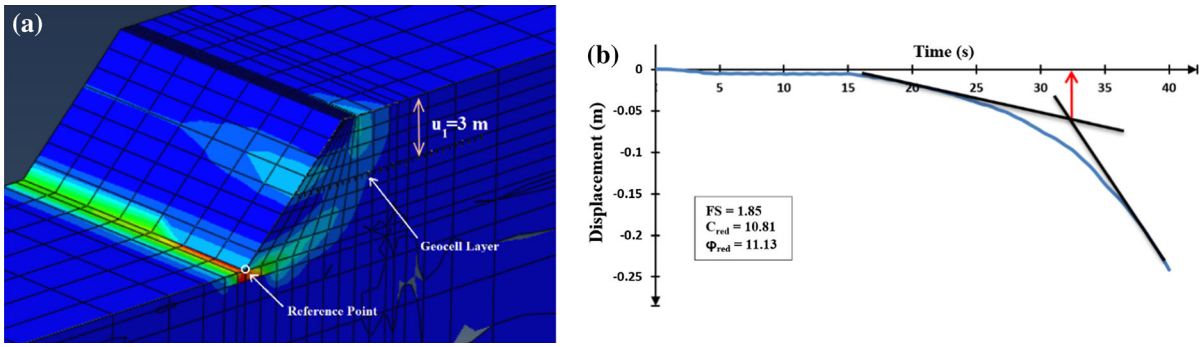

Fig. 6 Outputs of SRM analysis on the slope with β = 45° and H = 6 m, reinforced in the middle (u_1 = 3 m). **a** A 3D section showing the geocell layer placement and slip surface. **b** Displacement–time graph

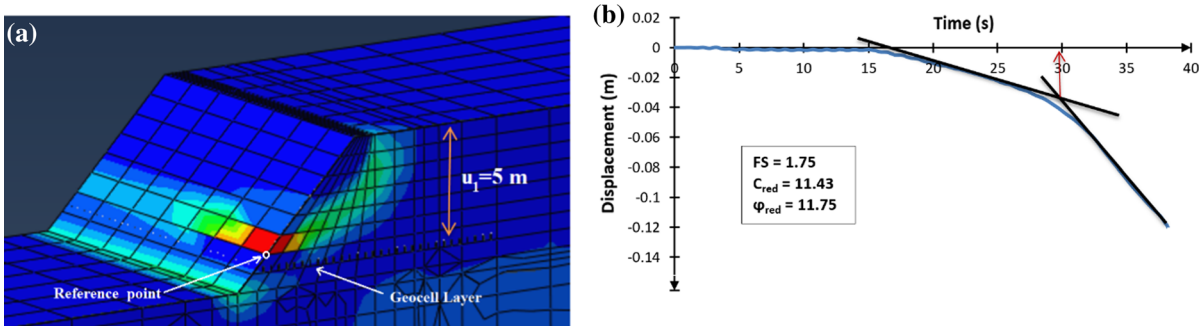

Fig. 7 Outputs of SRM analysis on the slope with β = 45° and H = 6 m, reinforced in the bottom (u_1 = 5 m). **a** A 3D section showing the geocell layer placement and slip surface. **b** Displacement–time graph

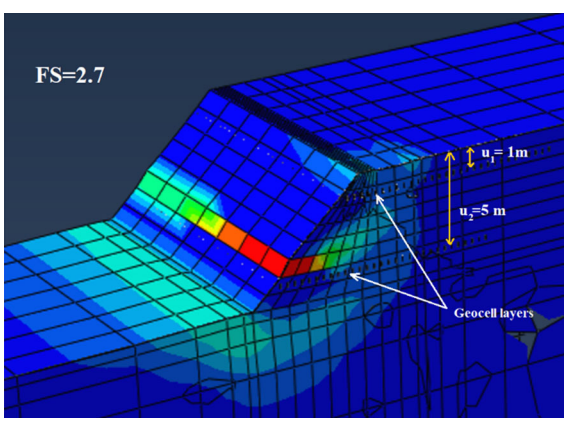

Fig. 8 A 3D section of the double layer geocell reinforced slope on the verge of failure (β = 45°)

distributed pattern (u_1 = 1 m, s = 2.2 m) and bottom-inclined pattern (u_1 = 2.4 m, s = 1.5 m) were created. Results of the analyses carried out to find the safety factor of the prementioned cases are summarized in Table 5 and corresponding failure surfaces are depicted in Fig. 8.

As Table 5 suggests, equally distributed pattern is superior to the other two cases, although it is followed by the top-inclined pattern with just a slight difference in the factor of safety (less than 2%). Bot-inclined pattern gives rise to the lowest factor of safety mainly due to the vulnerability of the unreinforced soil mass above the first layer against failure as indicated in Table 5 (failure surface column) and the middle section presented in Fig. 9c.

In addition, practically 2D failure surfaces, extended to the side boundaries, formed in the case of top inclined and equally inclined geocell layers (Fig. 9a, b) show that the stepwise transmission of local load intensity from the top geocell layer to the underlying layers has significantly undermined the role of the local load in the failure. Hence, in these situations, self-weight of the slope is the primary contributing factor to failure rather than the local load. On the contrary, due to the relatively great distance between the ground surface, where the local load is placed, and the uppermost geocell layer, a three

Table 5 Results of the analyses on different three-layer geocell patterns

Pattern	u_1 (m)	s (m)	u_2 (m)	u_3 (m)	Failure surface	FS
Top-inclined	1	1.5	2.7	4.4	Below the lowest layer	2.75
Equally distributed	1	2.2	3.4	5.8	Between the second and third layers	2.8
Bot-inclined	2.4	1.5	4.1	5.8	Above the first layer	2.1

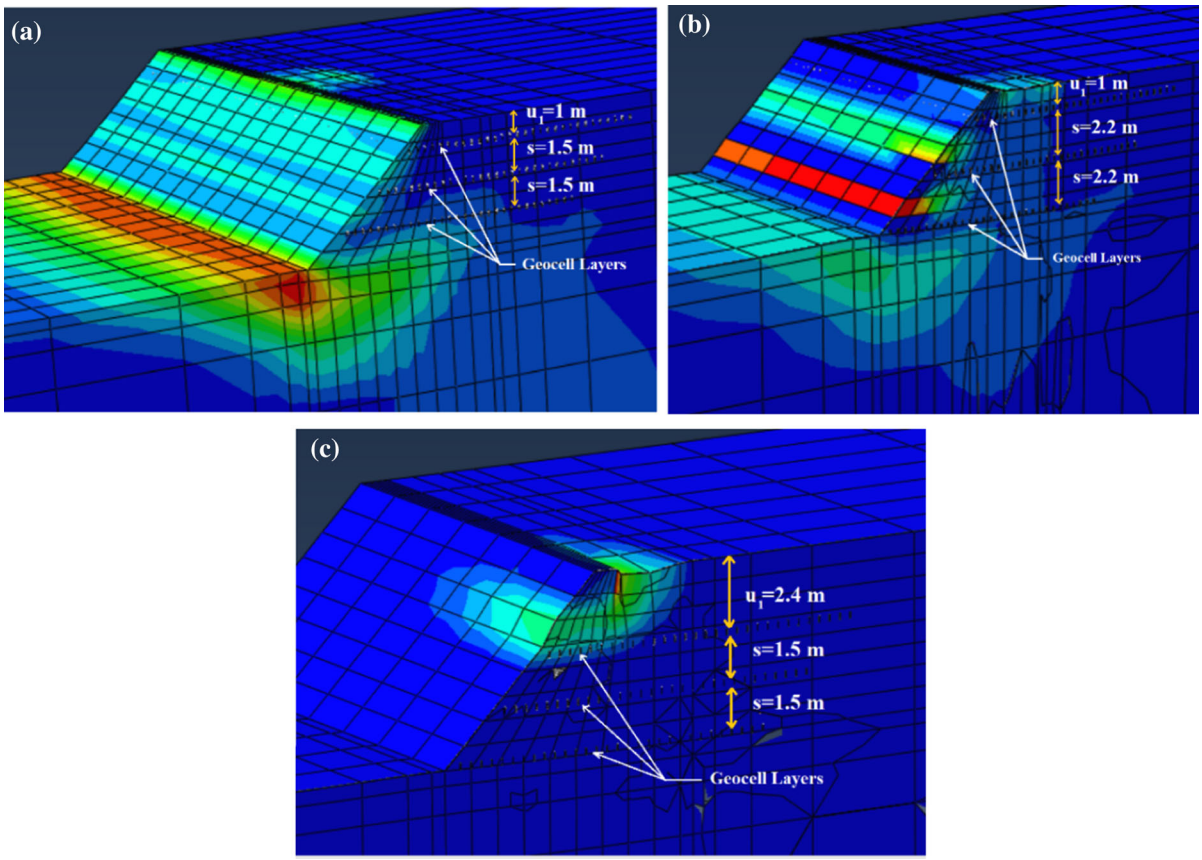

Fig. 9 Effect of distribution layout of reinforceing layers on a typical slope reinforced with thrre geocell layers. **a** Layers mainly on upper part of the slope (overall view), **b** equally distributed layers over the slope height (midle section) and **c** layers mainly on lower part of the slope (middle section)

dimensional failure surface is created in the case of bot-inclined pattern (Fig. 9c).

Looking through the results of the two and three layer geocell reinforcement, it can be argued that the geocell layer establishes a stiff platform for the overlying mass to distribute its weight more uniformly over a wider area. This way, it prevents the failure surface from penetrating into the mass below the geocell layer. However, if the unreinforced soil masses above the topmost geocell layer, between the two successive layers and below the lowermost layer are high enough, failure might take place in those regions. Therefore, altering the depth of the first layer (u_1) and the distance between the lower layers (s) is of central importance for an optimal design.

5.2 Effect of Number of Geocell Layers and Slope Angle

Certainly, an increase in the number of reinforcing layers boosts the stability of slopes. However, rate of stability enhancement is of great concern and helps designers to reach a more reasonable and cost effective pattern. In this study the same 45° slope considered in the previous sections was reinforced with one, three and five geocell mattresses respectively (n = 1, n = 3 and n = 5) and the factor of safety was determined for each situation following the prescribed stepped procedure. Besides, to see the influence of the slope angle, the reinforcement patterns just described were also considered for a model study with β = 75°. In order to ease judgment, the top reinforcing layer for all three cases is planted at u_1 = 1 m and the lowermost geocell layer for both n = 3 and n = 5 is assumed at the slope toe (u = 5.8 m). The distance between middle geocell layers was selected so that the equally spaced pattern was created. In this regard, s = 1 m and a = 2.2 m were considered for n = 5 and n = 3 respectively. The factor of safety versus the number of reinforcement layers is illustrated in Fig. 9.

As shown by Fig. 10, the number of geocell layers is effective in the FS enhancement only up to a certain level. For the cases considered in the current study, adding geocell layers in excess of n = 3 is practically useless regardless of the slope angle. For β = 45°, the factor of safety follows an increasing trend from n = 0 to n = 3. The same is not always the case for β = 75° as the marginal rise in FS value between n = 0 and n = 1 indicates in Fig. 10. The foregoing phenomenon can be argued with the aid of Fig. 11.

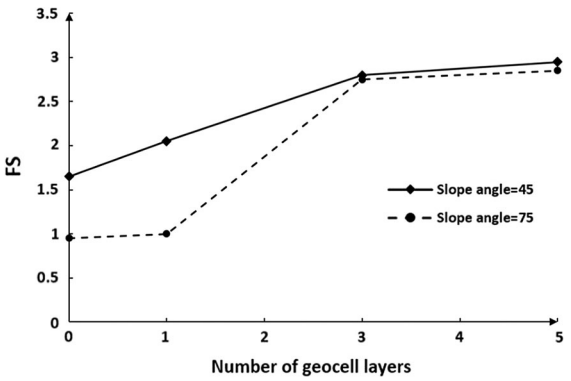

Fig. 10 Effect of the number of geocell layers and slope angle on FS

There is no tangible difference between the shape of the slope failure associated with n = 0 (Fig. 11a) and that of n = 1 (Fig. 11b). It seems that due to the steepness of the slope with β = 75°, the slope self-weight is the leading contributing factor to failure as opposed to β = 45° for which the surface loading plays the key role in the slope instability and the induced uniformity of load by the top geocell layer is significant for the stability of slope. Therefore, it can be expected that installation of the reinforcement on top of the slope will not lead to a considerable change in FS since the self-weight negatively alters the relatively large unreinforced part below the geocell mattress.

In addition, the great improvement in the safety of the steeper slope, β = 75°, for n > 1can be justified with the presented arguments. As Fig. 10 indicates, reinforcing the 75° slope with three or more geocell layers has led to the factors of safety close to those of β = 45°. This obviously introduces the geocell reinforcement as a robust method for enhancing the stability of the steep slopes.

It should be noted that the temperature dependent strength parameters assigned to the soil in ABAQUS and introduced in Table 2 were extended to involve the factors of safety smaller than unity like FS = 0.95 for unreinforced steep slope (β = 75°) indicated in Fig. 10.

6 Conclusions

Even if the geometry, material and loading of the geocell-reinforced slopes can be regarded as symmetric, due to honeycomb structure of geocells, three dimensional analysis is inevitable to have accurate insight into the stability of such slopes. Therefore, geocells in their original 3D shape were modeled inside the slope bodies as reinforcing elements and were analyzed by the finite element software ABAQUS. Because of the inability of ABAQUS in performing SRM analysis directly, a step by step SRM procedure was adopted to obtain the factor of safety of geocell-reinforced slopes. Then, effects of some significant contributing parameters such as the depth of geocell mattresses, the pattern of multilayer reinforcement and the number of geocell layers on FS were investigated through some problem solving. All investigated slopes were subjected to certain

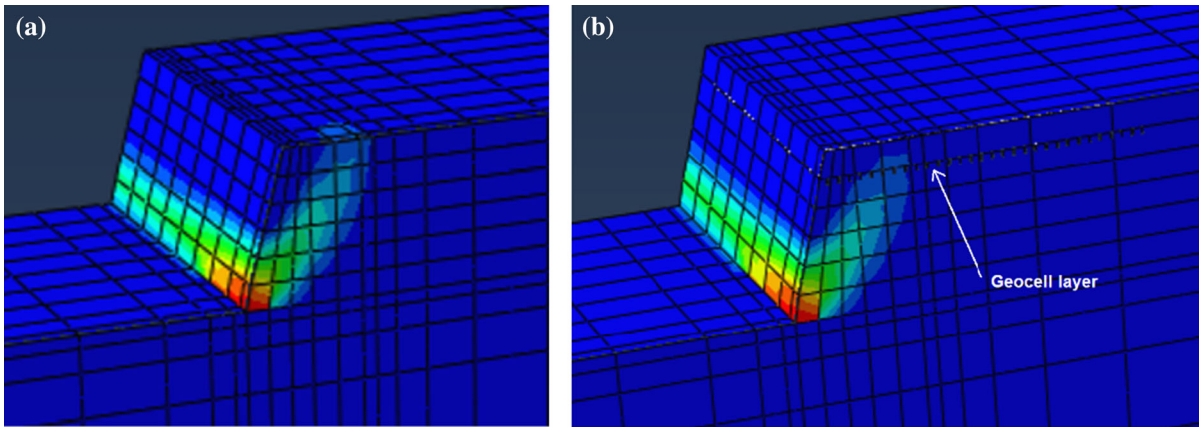

Fig. 11 Cross section of the slope with β = 75° and L/B = 2 on the verge of failure for: **a** unreinforced case, **b** reinforced on top with a single geocell layer (u_1 = 1 m)

rectangular (L/B = 2) uniform pressure (q = 100 kPa) on their crest. The following are the leading findings of the present study:

1. Factors of safety obtained by the stepped SRM procedure proposed in this study, showed acceptable compliance with the results of a previous study on the stability of unreinforced slopes by finite difference SRM using FLAC3D.
2. Effect of the placement depth on the stability of 45° slopes reinforced with single geocell layer indicates that reinforcement of slopes at top, middle and bottom gives rise to the highest, moderate and the lowest FS respectively. Inspection of the slip surfaced associated with each of the described cases showed that the lower FS obtained for bot-reinforcement is attributable to a large unreinforced soil mass left above the reinforcing layer.
3. Adding one layer of geocell at the bottom of a certain slope in excess of the top-reinforcing layer resulted in 32% increase in FS.
4. Equally distributed geocell layers were shown to be the optimal pattern, in terms of FS, among the three different three-geocell-layer reinforced slopes considered herein. The other two patterns, namely layers inclined toward the top of the slope and layers inclined to the bottom of the slope were found to have the middle and the minimal factor of safety respectively.
5. Analysis on the slopes stabilized by n number of geocell layers (n = 0,1, 3, 4, 5) revealed that the increase in the number of geocell layers is no longer effective beyond a certain value of n. For two cases investigated here (β = 45°, 75°), safety factor leveled off beyond n = 3.
6. For the steep slope considered herein (β = 75°), top geocell reinforcement has only a marginal effect on FS compared to unreinforced case. Inspecting the corresponding slip surfaces, it was concluded that self-weight is the main factor contributing factor to the failure. Thus, strengthening such slopes at the bottom by geocell layer is more effective compared to what was observed for a slope that is less steep (β = 45°).

References

Ahmed A, Ugai K, Yang QQ (2012) Assessment of 3D slope stability analysis methods based on 3D simplified Janbu and Hovland methods. Int J Geomech 12(2):81–89

Bathurst RJ, Karpurapu R (1993) Large-scale triaxial compression testing of geocell-reinforced granular soils. Geotech Test J 16(3):296–303

Biswas A, Krishna AM (2017) Geocell-reinforced foundation systems: a critical review. Int J Geosynth Ground Eng 3(2):17

Cai F, Ugai K (2000) Numerical analysis of the stability of a slope reinforced with piles. Soils Found 40(1):73–84

Cai F, Ugai K (2003) Reinforcing mechanism of anchors in slopes: a numerical comparison of results of LEM and FEM. Int J Numer Anal Meth Geomech 27(7):549–564

Chen Z, Mi H, Zhang F, Wang X (2003) A simplified method for 3D slope stability analysis. Can Geotech J 40(3):675–683

Cheng YM, Yip CJ (2007) Three-Dimensional asymmetrical slope stability analysis extension of Bishop's, Janbu's, and

Morgenstern–Price's techniques. J Geotech Geoenviron Eng 133(12):1544–1555
Cheng YM, Lansivaara T, Wei WB (2007) Two-dimensional slope stability analysis by limit equilibrium and strength reduction methods. Comput Geotech 34(3):137–150
Dash SK, Krishnaswamy NR, Rajagopal K (2001) Bearing capacity of strip footings supported on geocell-reinforced sand. Geotext Geomembr 19(4):235–256
Dash SK, Sireesh S, Sitharam TG (2003a) Behaviour of geocell-reinforced sand beds under circular footing. Proc Inst Civil Eng Ground Improv 7(3):111–115
Dash SK, Sireesh S, Sitharam TG (2003b) Model studies on circular footing supported on geocell reinforced sand underlain by soft clay. Geotext Geomembr 21(4):197–219
Dash SK, Rajagopal K, Krishnaswamy NR (2004) Performance of different geosynthetic reinforcement materials in sand foundations. Geosynth Int 11(1):35–42
Dash SK, Rajagopal K, Krishnaswamy NR (2007) Behaviour of geocell-reinforced sand beds under strip loading. Can Geotech J 44(7):905–916
Deng JH, Tham LG, Lee CF, Yang ZY (2007) Three-dimensional stability evaluation of a preexisting landslide with multiple sliding directions by the strength-reduction technique. Can Geotech J 44(3):343–354
Donald IB, Giam SK (1988) Application of the nodal displacement method to slope stability analysis. In: 5th Australia-New Zealand conference on geomechanics: prediction versus performance; preprints of papers. Institution of Engineers, Australia, p 456
Faheem H, Cai F, Ugai K, Hagiwara T (2003) Two-dimensional base stability of excavations in soft soils using FEM. Comput Geotech 30(2):141–163
Griffiths DV, Lane PA (1999) Slope stability analysis by finite elements. Geotechnique 49(3):387–403
Griffiths DV, Lu N (2005) Unsaturated slope stability analysis with steady infiltration or evaporation using elasto-plastic finite elements. Int J Numer Anal Meth Geomech 29(3):249–267
Griffiths DV, Marquez RM (2007) Three-dimensional slope stability analysis by elasto-plastic finite elements. Geotechnique 57(6):537–546
Han J, Yang X, Leshchinsky D, Parsons R (2008) Behavior of geocell-reinforced sand under a vertical load. Transp Res Record J Transp Res Board 2045:95–101
Hegde A (2017) Geocell reinforced foundation beds-past findings, present trends and future prospects: a state-of-the-art review. Constr Build Mater 154:658–674
Hegde AM, Sitharam TG (2015) Effect of infill materials on the performance of geocell reinforced soft clay beds. Geomech Geoeng 10(3):163–173
Hungr O (1987) An extension of Bishop's simplified method of slope stability analysis to three dimensions. Geotechnique 37(1):113–117
Lam L, Fredlund DG (1993) A general limit equilibrium model for three-dimensional slope stability analysis. Can Geotech J 30(6):905–919
Latha GM, Dash SK, Rajagopal K (2008) Equivalent continuum simulations of geocell reinforced sand beds supporting strip footings. Geotech Geol Eng 26(4):387
Leshchinsky B, Ling H (2013a) Effects of geocell confinement on strength and deformation behavior of gravel. J Geotech Geoenviron Eng 139(2):340–352
Leshchinsky B, Ling HI (2013b) Numerical modeling of behavior of railway ballasted structure with geocell confinement. Geotext Geomembr 36:33–43
Lin H, Xiong W, Cao P (2013) Stability of soil nailed slope using strength reduction method. Eur J Environ Civil Eng 17(9):872–885
Madhavi Latha G, Rajagopal K (2007) Parametric finite element analyses of geocell-supported embankments. Can Geotech J 44(8):917–927
Mandal JN, Gupta P (1994) Stability of geocell-reinforced soil. Constr Build Mater 8(1):55–62
Matsui T, San KC (1992) Finite element slope stability analysis by shear strength reduction technique. Soils Found 32(1):59–70
Mehdipour I, Ghazavi M, Moayed RZ (2013) Numerical study on stability analysis of geocell reinforced slopes by considering the bending effect. Geotext Geomembr 37:23–34
Mehdipour I, Ghazavi M, Ziaie Moayed R (2017) Stability analysis of geocell-reinforced slopes using the limit equilibrium horizontal slice method. Int J Geomech 17(9):06017007
Rajagopal K, Krishnaswamy NR, Latha GM (1999) Behaviour of sand confined with single and multiple geocells. Geotext Geomembr 17(3):171–184
Rawat S, Gupta AK (2016) Analysis of a nailed soil slope using limit equilibrium and finite element methods. Int J Geosynth Ground Eng 2(4):34
Sireesh S, Sitharam TG, Dash SK (2009) Bearing capacity of circular footing on geocell–sand mattress overlying clay bed with void. Geotext Geomembr 27(2):89–98
Sitharam TG, Sireesh S, Dash SK (2005) Model studies of a circular footing supported on geocell-reinforced clay. Can Geotech J 42(2):693–703
Song E (1997) Finite element analysis of safety factor for soil structures. Chin J Geotech Eng 19(2):1–7
Tafreshi SM, Dawson AR (2012) A comparison of static and cyclic loading responses of foundations on geocell-reinforced sand. Geotext Geomembr 32:55–68
Tschuchnigg F, Schweiger HF, Sloan SW (2015) Slope stability analysis by means of finite element limit analysis and finite element strength reduction techniques. Part I: numerical studies considering non-associated plasticity. Comput Geotech 70:169–177
Ugai K, Leshchinsky DOV (1995) Three-dimensional limit equilibrium and finite element analyses: a comparison of results. Soils Found 35(4):1–7
Wei WB, Cheng YM (2009) Strength reduction analysis for slope reinforced with one row of piles. Comput Geotech 36(7):1176–1185
Wei WB, Cheng YM (2010) Soil nailed slope by strength reduction and limit equilibrium methods. Comput Geotech 37(5):602–618
Wei WB, Cheng YM, Li L (2009) Three-dimensional slope failure analysis by the strength reduction and limit equilibrium methods. Comput Geotech 36(1):70–80
Wong FS (1984) Uncertainties in FE modeling of slope stability. Comput Struct 19(5–6):777–791

Zhang L, Zhao M, Shi C, Zhao H (2010) Bearing capacity of geocell reinforcement in embankment engineering. Geotext Geomembr 28(5):475–482

Zienkiewicz OC, Humpheson C, Lewis RW (1975) Associated and non-associated visco-plasticity and plasticity in soil mechanics. Geotechnique 25(4):671–689